Positron-induced emission of electron–positron pairs from solid surfaces

2009 J. Phys.: Condens. Matter 21 355002

(http://iopscience.iop.org/0953-8984/21/35/355002)

IOP PUBLISHING JOURNAL OF PHYSICS: CONDENSED MATTER

J. Phys.: Condens. Matter **21** (2009) 355002 (12pp) doi:10.1088/0953-8984/21/35/355002

Positron-induced emission of electron–positron pairs from solid surfaces

F Giebels, H Gollisch and R Feder

Theoretische Festkörperphysik, Universität Duisburg-Essen, D-47048 Duisburg, Germany

Received 6 April 2009, in final form 7 April 2009
Published 20 July 2009
Online at stacks.iop.org/JPhysCM/21/355002

Abstract

The collision of a low-energy positron, which impinges on a crystalline surface, with a valence electron may result in the emission of a spatially separated time-correlated electron–positron pair. We present a method for calculating the cross section for this positron surface reaction channel, which we briefly refer to as (p, ep) in analogy to electron-induced pair emission (e, 2e). The two-particle final state is represented by a product of an electron and a positron diffraction state coupled by a 'correlation factor', which accounts for the screened Coulomb interaction. The electron–solid and positron–solid quasi-particle potentials are based on first-principles calculations within density functional theory. Numerical (p, ep) results are presented for Cu(111) and compared to their (e, 2e) counterparts. Energy distributions for constant emission angles reflect, to a large extent, the valence electron density of states. In equal-energy (p, ep) angular distributions, the Coulomb interaction produces a central accumulation zone—in contrast to a depletion zone for (e, 2e)—the relative weight and the extension of which are subject to 'matrix element effects'. At larger angles sharp features arise from single-particle surface resonances.

(Some figures in this article are in colour only in the electronic version)

1. Introduction

The use of positrons in solid state and surface physics has a long-standing tradition (cf, e.g., reviews [1–3] and references therein). For a low-energy positron beam impinging on a surface, well-known and intensively studied reaction channels include in particular low-energy positron diffraction (LEPD), re-emission after thermalization and pair annihilation.

In a recent pioneering experiment [4], a new reaction channel has been made accessible: the momentum-resolved measurement of a spatially separated time-correlated electron–positron pair, which is emitted from a crystalline surface, has been demonstrated to be feasible. This opens a new way of obtaining information on the correlation between positrons and electrons. Since positrons and electrons are distinguishable particles, the pair correlation in positron-induced electron–positron emission (referred to in brief in the following as (p, ep)) is solely due to the Coulomb interaction. This is in contrast to the established technique of electron-induced electron–electron emission (e, 2e) (cf [5–11] and references therein) in the hitherto used set-ups without spin analysis, in which the pair correlation arises from a combination of the Coulomb interaction and the exchange interaction.

On the theoretical side, a general many-body expression for the (p, ep) reaction cross section from crystal surfaces has previously been given [12] and evaluated in a low-order multiple scattering expansion, yielding in particular insight into pair diffraction effects and into the principal differences between (p, ep) and (e, 2e).

In the present work, we calculate the (p, ep) reaction cross section from crystal surfaces in a more realistic way, which goes beyond the earlier work [12] in the following respects:

(a) the electron–solid and positron–solid interaction potentials are derived from first-principles electronic structure calculations within density functional theory, with the positron–solid potential containing an attractive correlation part, which (at low energies) is about six times stronger than that of the electron–solid potential;
(b) for these potentials, multiple scattering is taken into account fully, i.e. we have low-energy electron diffraction (LEED) and low-energy positron diffraction (LEPD) states;
(c) the electron–positron two-particle final state is represented by a product of an LEED and an LEPD state coupled by a 'correlation factor', which is obtained by solving

the relative-particle equation containing the screened electron–positron interaction.

Numerical (p, ep) results are presented for Cu(111), with an emphasis on the manifestation of the Coulomb correlation and its interplay with matrix element effects in angular distributions. Comparison with their counterparts for (e, 2e) with definite opposite spins, i.e. in the absence of exchange, shows massive differences which are due to different single-particle potentials and a stronger Coulomb correlation. For spin-unresolved (e, 2e), additional differences arise from the exchange interaction.

Our paper is organized as follows. In section 2 we present a general (p, ep) reaction cross-section expression and two fundamental ingredients needed for evaluating it: (a) the two-particle wavefunction of a positron and an electron coupled by the bare or a screened Coulomb interaction, illustrated graphically by the pair correlation function between a plane-wave positron and a plane-wave electron (section 2.2) and (b) the single quasi-particle potentials describing the positron–crystal and the electron–crystal interaction (section 2.3). In section 3 we present, for the Cu(111) surface, numerically calculated (p, ep) energy and angular distributions and compare them to their counterparts in (e, 2e) with and without spin resolution.

2. Theory

2.1. Reaction cross section

For a positron with low energy E_1, surface-parallel momentum $\vec{k}_1^{\parallel}$ and spin σ_1 incident on a crystalline surface, the reaction cross section for the correlated emission of a positron with energy E_3, surface-parallel momentum $\vec{k}_3^{\parallel}$ and spin σ_3 and an electron with energy E_4, surface-parallel momentum $\vec{k}_4^{\parallel}$ and spin σ_4 can be written as

$$I^{\sigma_1}_{\sigma_3,\sigma_4} = \frac{k_3 k_4}{k_1} \sum_{\sigma_2} \langle 3,4|U|1\rangle \left(-\frac{1}{\pi}\right) \times \operatorname{Im} G_2^r(E_2, \vec{k}_2^{\parallel}, \sigma_2) \langle 1|U|3,4\rangle, \quad (1)$$

which is formally the same as the expression for the reaction cross section for electron-induced electron pair emission (e, 2e), which has been previously derived and discussed in detail (cf the review article [5] and references therein). In equation (1) $|1\rangle$ is a low-energy-positron-diffraction (LEPD) state with quantum numbers set asymptotically by the positron gun. G_2^r is the spin- and $\vec{k}^{\parallel}$-resolved valence electron Green function with $E_2 = E_3 + E_4 - E_1$ and $\vec{k}_2^{\parallel} = \vec{k}_3^{\parallel} + \vec{k}_4^{\parallel} - \vec{k}_1^{\parallel} + \vec{g}^{\parallel}$ such that energy and surface-parallel momentum modulo a surface reciprocal lattice vector $\vec{g}^{\parallel}$ are conserved. U denotes the attractive screened Coulomb interaction between positron and electron. $|3,4\rangle$ is the U-correlated positron–electron final state with boundary conditions such that a positron with energy E_3 and surface-parallel momentum component $\vec{k}_3^{\parallel}$ arrives at one detector and an electron with E_4 and $\vec{k}_4^{\parallel}$ at the other detector.

While equation (1) is formally identical for (p, ep) and (e, 2e), its further evaluation for (p, ep) differs strongly from that for (e, 2e) in two main respects: (a) correlation and (absence of) exchange in the two-particle state $|3,4\rangle$ and (b) the effective single-positron potential, which determines the LEPD states. In the following, we focus on these two problems in (p, ep).

2.2. Electron–positron pair correlation

The correlated electron–positron state $|3,4\rangle$ in equation (1) is an eigenstate of the two-particle Hamiltonian:

$$H = H_{\mathrm{p}} + H_{\mathrm{e}} + U, \quad (2)$$

where U is the electron–positron interaction, and H_{p} and H_{e} are two single-particle Hamiltonians with effective single-particle potentials V_{p} and V_{e}, which represent the interaction of the positron and the electron with the semi-infinite crystalline solid. Our method of calculating positron–electron states is analogous to the one which we have developed for correlated two-electron states and presented in detail [7]. In this section, we therefore only outline some essential features of the method and then illustrate the electron–positron pair correlation by numerical results.

Denoting the eigenfunctions of H_{p} and H_{e} in equation (2) by $\varphi_{\mathrm{p}}(\vec{r}_1)$ and $\varphi_{\mathrm{e}}(\vec{r}_2)$, respectively, the eigenstate $\phi(\vec{r}_1, \vec{r}_2)$ of H is expressed in the form

$$\phi(\vec{r}_1, \vec{r}_2) = \varphi_{\mathrm{p}}(\vec{r}_1)\varphi_{\mathrm{e}}(\vec{r}_2) f^{\mathrm{c}}(\vec{r}_1, \vec{r}_2), \quad (3)$$

where $f^{\mathrm{c}}(\vec{r}_1, \vec{r}_2)$ is a 'Coulomb correlation factor'. In the absence of Coulomb interaction, i.e. for $U = 0$, $f^{\mathrm{c}} = 1$, and the two-particle state is simply a product of two single-particle states.

The single-particle states φ_{p} and φ_{e} are (time-reversed) LEPD and LEED states, respectively, and $f^{\mathrm{c}}(\vec{r}_1, \vec{r}_2)$ is approximated by the correlation factor $f^{\mathrm{c}}(\vec{r}; \vec{k})$ between two plane waves $\exp(\mathrm{i}\vec{k}_1\vec{r}_1)$ and $\exp(\mathrm{i}\vec{k}_2\vec{r}_2)$ with relative coordinate $\vec{r} = \vec{r}_1 - \vec{r}_2$ and relative momentum $\vec{k} = \vec{k}_1 - \vec{k}_2$. For a given repulsive or attractive central potential $U(r)$ (e.g. a screened Coulomb potential inside the solid) $f^{\mathrm{c}}(\vec{r}; \vec{k})$ is calculated numerically by solving the Schrödinger equation (in atomic units with energy in Hartree)

$$\left(-\frac{1}{m}\Delta + U(r)\right)\varphi(\vec{r}; \vec{k}) = \frac{k^2}{4m}\varphi(\vec{r}; \vec{k}) \quad (4)$$

for the relative-particle wavefunction $\varphi(\vec{r}; \vec{k}) := \mathrm{e}^{\mathrm{i}\frac{1}{2}\vec{k}\vec{r}}\, f^{\mathrm{c}}(\vec{r}; \vec{k})$.

Before showing some numerical results, we point out that our correlation factor $f^{\mathrm{c}}(\vec{r}; \vec{k})$ is closely related to the two-particle density $\rho(\vec{r}_1, \vec{r}_2)$ in the case that the single-particle states φ_{p} and φ_{e} are plane waves. From equation (3) one then obtains

$$\rho(\vec{r}_1, \vec{r}_2) = |f^{\mathrm{c}}(\vec{r}; \vec{k})|^2. \quad (5)$$

Since the single-particle densities are normalized to unity, this is identical with the pair correlation function, i.e. the probability of finding the electron at $\vec{r}_2$ if the positron is at $\vec{r}_1$. In the case of two plane-wave electrons with anti-parallel spins, the corresponding $|f^{\mathrm{c}}(\vec{r}; \vec{k})|^2$ can be understood as the probability of finding an electron with spin $|-s\rangle$ at $\vec{r}_2$ if an electron with fixed spin $|s\rangle$ is at $\vec{r}_1$ (cf [7]).

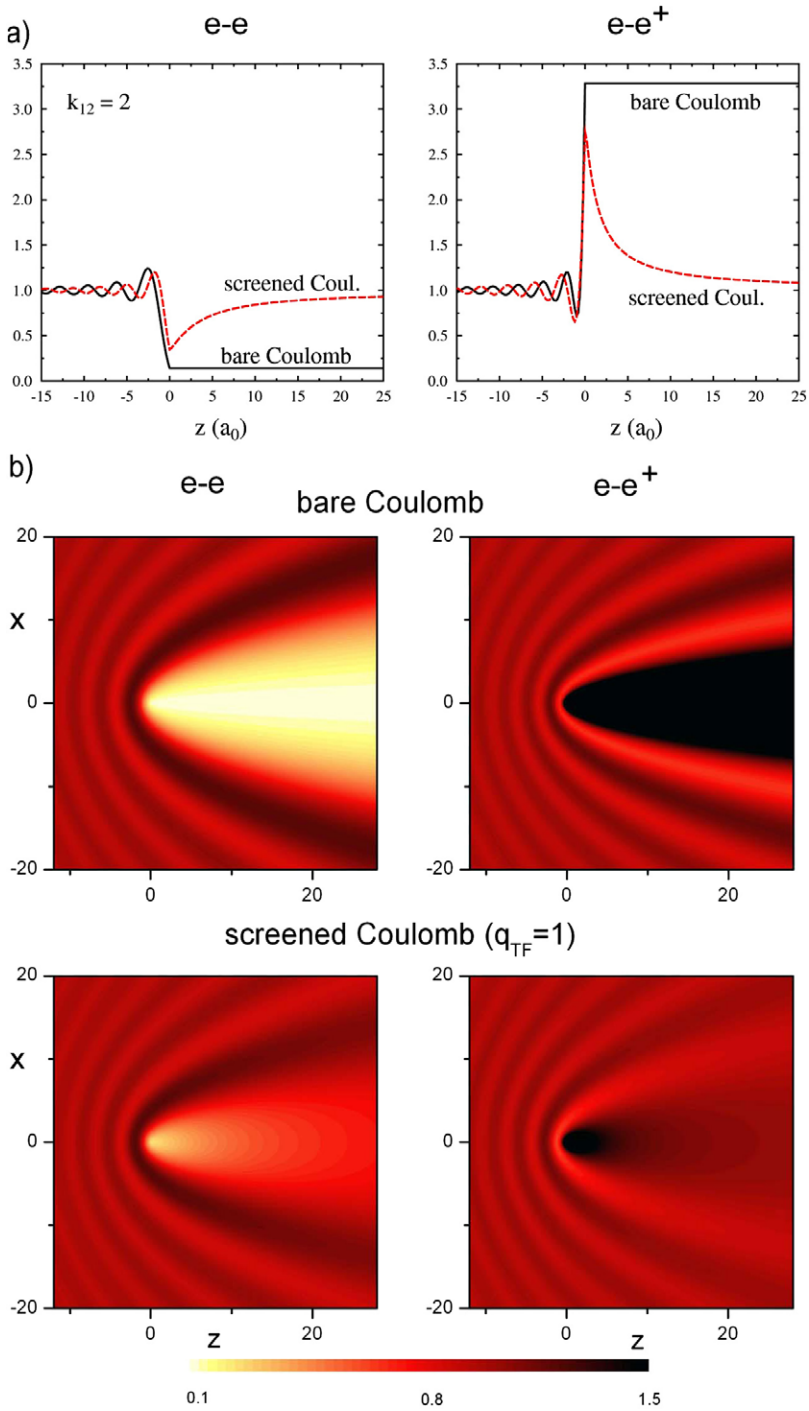

Figure 1. Pair correlation function $\rho(\vec{r}_1 = 0, \vec{r}_2 = \vec{r}) = |f^c(\vec{r}; \vec{k})|^2$ (cf equation (5)) between two plane-wave electrons of fixed anti-parallel spins (left-hand panels) and between a plane-wave positron and a plane-wave electron (right-hand panels) with relative momentum $\vec{k} = \vec{k}_1 - \vec{k}_2$ along the z axis. (a) $|f^c(x = 0, y = 0, z; k = 2)|^2$ for bare Coulomb interaction (solid (black) line) and for a Thomas–Fermi-screened Coulomb interaction $\pm\exp(-q_{TF}r)/r$ with $q_{TF} = 1$ (in atomic units) (dashed (red) line). (b) Contour plots of $|f^c(x, y = 0, z; k = 2)|^2$ for bare (top panels) and for Thomas–Fermi-screened (bottom panels) Coulomb interaction.

In figure 1 we show, for the bare Coulomb potential $\pm 1/r$ and for a screened one $\pm\exp(-q_{TF}r)/r$ in the Thomas–Fermi approximation, the dependence of the pair correlation function $\rho(\vec{r}_1 = 0, \vec{r}_2 = \vec{r}) = |f^c(\vec{r}; \vec{k})|^2$ (equation (5)) of an electron–positron pair and an anti-parallel spin electron–electron pair on x and z for a fixed momentum difference $\vec{k} = (0, 0, k)$ along the z axis. Since the correlation must be maximal for $\vec{r}_1 = \vec{r}_2$, i.e. $\vec{r} = \vec{r}_1 - \vec{r}_2 = 0$, it is immediately plausible that $|f^c(\vec{r}; \vec{k})|^2$ exhibits at $\vec{r} = 0$ a maximum in the 'attractive case' of the electron–positron pair and a minimum in the 'repulsive case' of the electron–electron pair.

The spatial dependence of $|f^c|^2$ can be semi-quantitatively understood by noting that $|f^c| = |\varphi|$ (cf equation (4)) and by approximating the relative-particle wavefunction φ by a

function $\tilde{\varphi}$ composed of an incident wave and a scattered wave:

$$\tilde{\varphi}(\vec{r}) = \mathrm{e}^{\mathrm{i}\kappa z} + F(\Theta)\mathrm{e}^{\mathrm{i}\kappa r}/r \tag{6}$$

where $\kappa = k/2$, F is a scattering amplitude and Θ the scattering angle (defined with respect to the positive z axis). Obviously, $\tilde{\varphi}$ is rotationally symmetric about the z axis. For $x = 0$ and $y = 0$, the z dependence is easily evaluated further. In the negative z direction we have $\tilde{\varphi}(0, 0, z) = \exp(-\mathrm{i}\kappa|z|)+F(\pi)\exp(\mathrm{i}\kappa|z|)/|z||\tilde{\varphi}|$. It thence oscillates with decreasing amplitude and with a wavelength $\pi/\kappa = 2\pi/k$. In the positive z direction $\tilde{\varphi}(0, 0, z) = \exp(-\mathrm{i}\kappa z)(1 + F(0)/z)$ and thence $|\tilde{\varphi}| = |1 + F(0)/z|$, i.e. going monotonically towards unity. The latter behaviour is seen in figure 1 for the screened potential, for which the approximation equation (6) is more appropriate than for the bare Coulomb potential. In summary, we thus have for $z < 0$ an oscillatory behaviour for both the electron–electron and the electron–positron pair, whereas in the half-space $z > 0$ there is a correlation hole in the electron–electron case and a correlation hill in the electron–positron case.

The complete spatial dependence of the pair correlation function $|f^{\mathrm{c}}(\vec{r}; \vec{k})|^2$ is implicit in the (x, z) plane contour plot in figure 1(b), since $|f^{\mathrm{c}}(\vec{r}; \vec{k})|^2$ is rotationally symmetric about the z axis for the present choice of $\vec{k} = (0, 0, k)$. As can be seen from figure 1(b), the maximal height of the electron–positron correlation hill is larger than the maximal depth of the electron–electron correlation hole. This is possible due to the fact that the probability density for finding two electrons at $r = 0$ cannot be less than zero, whereas for the probability density for an electron and a positron there is no obvious upper limit. This difference in the strength of the correlation between two electrons on the one hand and a positron and an electron on the other hand becomes even more pronounced for smaller k, as is demonstrated by figure 2.

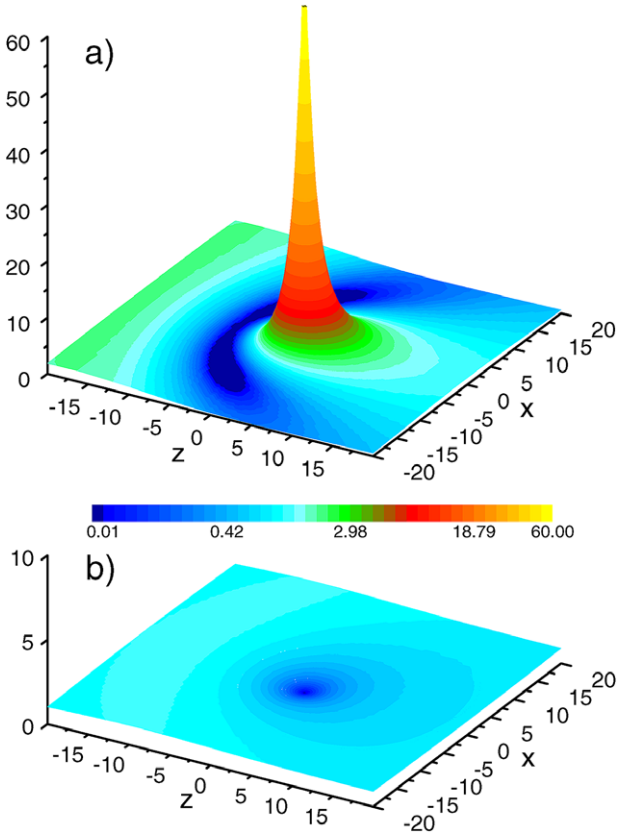

Figure 2. Pair correlation function $|f^{\mathrm{c}}(x, y = 0, z; k = 0.2)|^2$ (cf equation (5)) for a Thomas–Fermi-screened Coulomb interaction with $q_{\mathrm{TF}} = 0.56$ Bohr^{-1}: (a) between a plane-wave positron and a plane-wave electron, (b) between two plane-wave electrons of fixed anti-parallel spins.

2.3. Single-particle potentials

In the following, we specify, for the case of the Cu(111) surface, the single-particle potentials required for calculating the four quasi-particle states, which enter, together with the Coulomb correlation factor f^{c} (cf equation (3), in the pair emission cross section (equation (1))).

As a common basis, we first performed a self-consistent calculation of the electronic structure of the ground state of Cu(111) within density functional theory by means of the full-potential linearized augmented plane-wave (FLAPW) program package FLEUR [13], using a nineteen-layer film geometry and a local density approximation (LDA) [14] for the exchange–correlation potential. We thus obtained charge density $\rho(\vec{r})$, Coulomb potential $V^-_{\mathrm{coul}}(\vec{r})$ and total potential $V^-_{\mathrm{tot}}(\vec{r}) = V^-_{\mathrm{coul}}(\vec{r}) + V^-_{\mathrm{xc}}(\vec{r})$, where $V^-_{\mathrm{xc}}(\vec{r})$ denotes the exchange–correlation part. Our calculated electron work function for Cu(111) is 5.20 eV, i.e. close to the experimental value 4.94 ± 0.3 eV [15]. The occupied bulk bands are in very good agreement with those from other self-consistent ground state calculations using the same LDA (cf [16] and references therein). Casting the shape-unrestricted ground state potential $V^-_{\mathrm{tot}}(\vec{r})$ into the muffin tin form and employing it in a layer-Kohn–Korringa–Rostoker (KKR) calculation yields practically the same bands. Compared to their counterparts determined experimentally by photoemission [16], the calculated sp-like bands agree fairly well but the d-bands are about 0.5 eV too high in energy.

A real effective potential for the occupied one-electron states in (p, ep) and (e, 2e) was therefore constructed from our self-consistent charge density $\rho(\vec{r})$ using a non-local density approximation [16]. The resulting bands are in good agreement with experiment. The real potential was augmented by an energy-dependent imaginary part $-0.05 - (E - E_{\mathrm{F}})^2/((E - E_{\mathrm{F}})^2 + 0.49)$ eV for the occupied states and $-0.08(E - E_{\mathrm{F}})$ eV for the LEED-like states.

In the vacuum region (in the half-space $z < 0$), where LDA ground state potentials fail to have the asymptotic image potential form, we used a local surface barrier model $V(z)$ (cf [17]), which has as adjustable parameters an image plane position z_1 and a matching plane position $z_2 < z_1$. For $z < z_2$, $V(z)$ has (in atomic units) the image form $1/(4(z - z_1))$. For $z_2 < z < 0$, $V(z)$ is a third-order polynomial such that it matches, up to the first derivative, and the image potential form at z_2 and the real inner potential $V_{0\mathrm{r}}$ at $z = 0$. The value of $V_{0\mathrm{r}}$ affects not only the height but also the shape of the barrier. It is, however, not an adjustable parameter but rather determined

by our ground state inner potential together with the above-mentioned real self-energy correction. The choice of z_1 and z_2 is guided by the near-surface form of the planar average of the ground state surface potential.

For the interaction of the positron with the semi-infinite crystal, we first constructed a shape-unrestricted ground state potential $V^+_{\rm tot}$ as the sum of a Coulomb potential, which is the sign-reversed Coulomb potential $V^-_{\rm coul}(\vec{r})$ from the electron ground state calculation and an attractive positron–electron correlation potential $V^+_{\rm corr}(\vec{r})$. The latter was constructed similarly as described in detail in previous work [18, 19], but based on the charge density $\rho(\vec{r})$ from our self-consistent FLAPW film calculation. Inside the solid, we employed, in local density approximation $V^+_{\rm corr}(\rho(\vec{r}))$, correlation energies of a positron in an electron gas of density ρ from a many-body calculation [20] in a convenient parametrized form [21]. These correlation energies agree well with more recent many-body calculations [22].

In the vacuum region, the actual positron potential $V^+_{\rm tot}(\vec{r})$ has, in contrast to a local density approximation form, image behaviour far from the surface and forms a 'correlation well' above the topmost atomic layer before joining the potential inside the solid. It hosts a Rydberg-like series of bound positron surface states, the lowest one of which has been observed at -2.8 eV (below the vacuum zero) for Cu(111) [23]. A potential, which satisfies these requirements, is provided by our above form $V(z)$ of the electron surface potential barrier, with suitable parameters z_1 and z_2 and a smooth transition to the bulk inner potential for a positron, which is, as we shall show below (in figure 3 and its context), much smaller than its counterpart for an electron.

Using the above $V^+_{\rm tot}(\vec{r})$ in an FLAPW/FLEUR [13] calculation of positron states, we obtained firstly the lowest positron bulk state of Cu(111) at 0.3 eV above the vacuum threshold, implying a positron work function of -0.3 eV close to the experimental value of -0.4 eV [23]. Secondly, the lowest-energy surface state is at -2.8 eV, in agreement with experiment [23]. While the latter value requires a special choice of our surface barrier parameters, the bulk state energies and thence the positron work function do not depend on the surface barrier model, i.e. arise from first principles (within the framework of the local density approximation).

Our total positron potential $V^+_{\rm tot}(\vec{r})$ is shown as a 3D plot in figure 3(a) and, together with its electrostatic and correlation parts $V^+_{\rm coul}(\vec{r})$ and $V^+_{\rm corr}(\rho(\vec{r}))$, along a line normal to the surface in figure 3(b). Inside the solid, the interstitial average of $V^+_{\rm tot}(\vec{r})$, which corresponds to the inner potential in a muffin tin approximation, is at 5.26 eV below the vacuum level, which is much less than its counterpart for an electron (12.91 eV). It is interesting to note that the positron correlation potential part $V^+_{\rm corr}(\rho(\vec{r}))$ is substantially stronger than the correlation potential for an electron. In particular, its interstitial average of -8.63 eV (cf figure 3(b)) is about six times larger than its electron counterpart (-1.4 eV). This is in line with our above finding (section 2.2) that the pair correlation function $|f^{\rm c}|^2$ for small r is much stronger for an electron–positron pair than for an electron–electron pair (cf figures 1 and 2).

The quasi-particle potentials for the two positron states (the incident and the emitted one) in the (p, ep) reaction cross

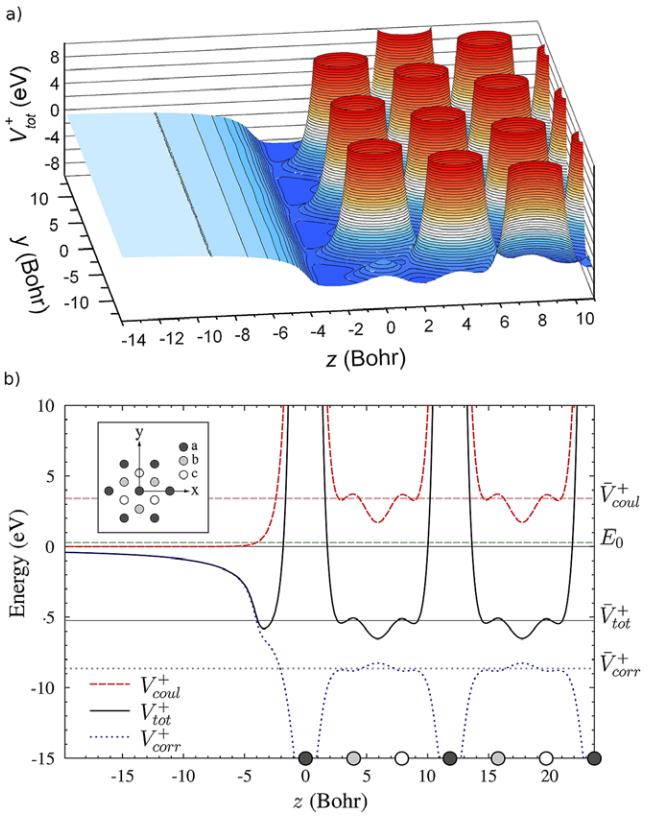

Figure 3. Positron potentials at the Cu(111) surface (relative to the vacuum zero): (a) 3D plot of the total potential $V^+_{\rm tot}(x = 0, y, z)$; the z axis is normal to the surface and the topmost internuclear plane is located at $z = 0$; x is along the $[1, -1, 0]$ direction and y along $[-1, -1, 2]$ (cf inset in figure 3(b)). (b) Total potential $V^+_{\rm tot}(x = 0, y = 0, z)$ (black solid line) and its constituent parts $V^+_{\rm coul}$ (red dashed line) and $V^+_{\rm corr}$ (blue dotted line). The corresponding horizontal lines mark the respective interstitial average potentials and the green dashed horizontal line indicates the energy E_0 of the lowest positron bulk state (0.3 eV above the vacuum level). Denoting the layer stacking parallel to the surface by (abc), the black-filled circles at the z axis indicate a layers, the grey-filled circles b layers and the empty circles c layers. Note that the chosen $(0, 0, z)$ line goes only through a nuclei.

section were constructed by first casting the above $V^+_{\rm tot}(\vec{r})$ into the muffin tin form, the latter yielding practically the same positron bulk band structure and work function as the full potential. Since the two relevant positron states are (except for the time reversal of the emitted state) the same as in low-energy positron diffraction (LEPD), we estimated the real self-energy correction by calculating LEPD spectra and comparing them to their experimental counterparts [24]. While a reduction of the real inner potential (corresponding to a reduction of the correlation potential) is inferred above about 60 eV, use of our original inner potential appears appropriate at energies below 30 eV for which we carried out pair emission calculations. The imaginary part of the effective potential has been estimated to be about twice as strong for a positron than for an electron [25]. With the latter as described above, we therefore used for the positrons the energy-dependent expression $-0.16(E - E_{\rm F})$ eV. Since the damping of the incident and the emitted positron state is thus stronger than in the electron case, one

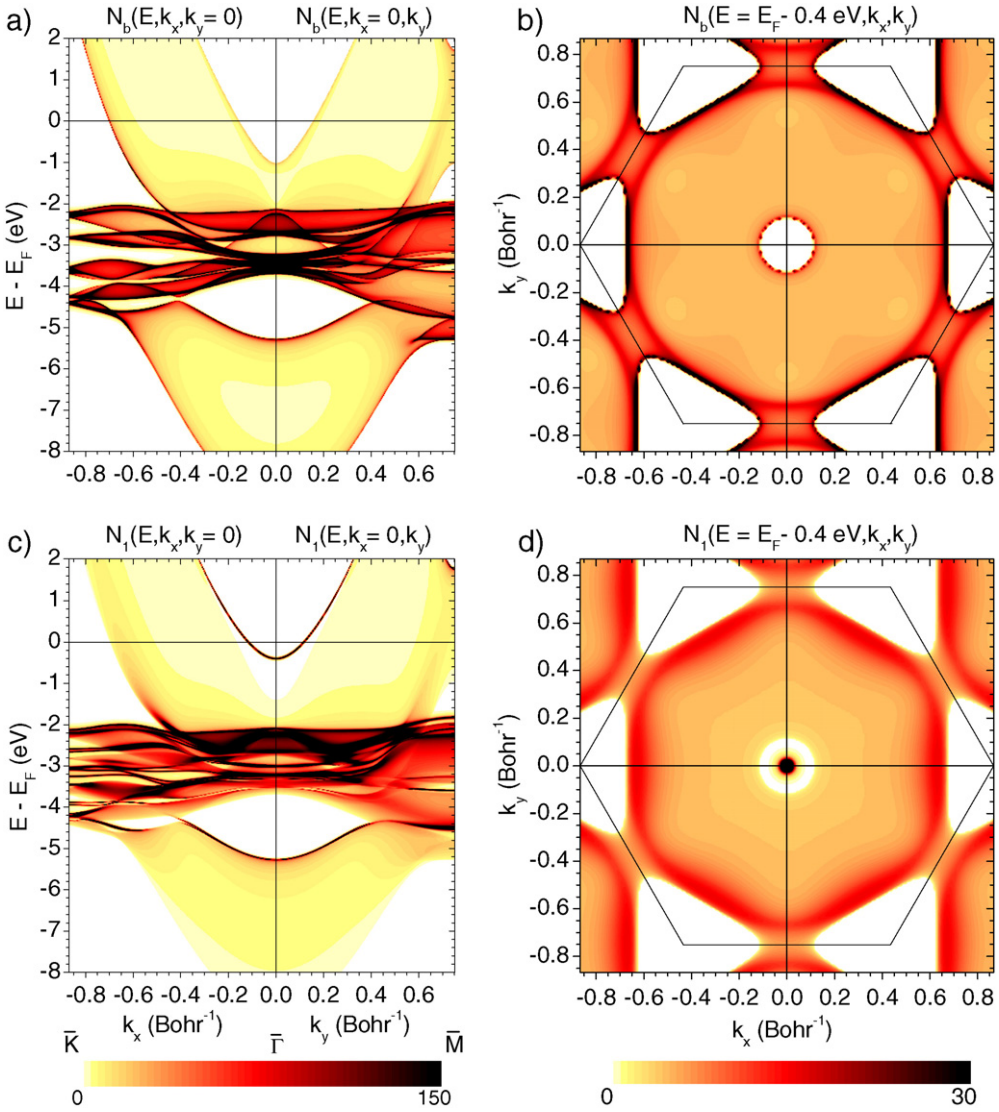

Figure 4. $\vec{k}^{\parallel}$- and layer-resolved density of initially occupied quasi-electron states $N_m(E, k_x, k_y)$ on Cu(111). To reveal more details, the imaginary potential part has been chosen as a very small constant (0.005 eV). (a) For bulk layer: $N_\mathrm{b}(E, k_x, k_y = 0)$ for $\vec{k}^{\parallel}$ along the $\overline{\Gamma}$–$\overline{\mathrm{K}}$ direction in the surface Brillouin zone (SBZ) and $N_\mathrm{b}(E, k_x = 0, k_y)$ for $\vec{k}^{\parallel}$ along $\overline{\Gamma}$–$\overline{\mathrm{M}}$. (b) For bulk layer: $N_\mathrm{b}(E, k_x, k_y)$ for fixed $E = E_\mathrm{F} - 0.4$ eV. The hexagon indicates the SBZ. (c) As (a) but N_1 for topmost (surface) layer. (d) As (b) but N_1 for topmost (surface) layer.

can expect (p, ep) to be generally more surface-sensitive than (e, 2e).

3. Pair emission results for Cu(111)

In the following, we present some typical positron-induced electron–positron pair emission (referred to in brief in the following as '(p, ep)') results calculated for Cu(111). We discuss them in comparison with corresponding (e, 2e) results and demonstrate the manifestation of the Coulomb correlation in the emitted pair.

As a prerequisite, it is useful to visualize (in figure 4) the initially bound electron states by means of the $\vec{k}^{\parallel}$- and layer-resolved density of occupied quasi-electron states (LDOS) $N_m(E, k_x, k_y)$, where m is the layer index. N_m has been calculated using the real effective electron potential, which we obtained from our FLAPW ground state charge density (cf section 2.3), augmented only by a very small imaginary part (0.005 eV) in order to reveal more details. The bulk LDOS shown in figures 4(a) and (b) corresponds to the projection of the bulk band structure onto the surface. In particular, in figure 4(a) the features at $\vec{k}^{\parallel} = 0$ reflect very closely the experimental and calculated bulk band structures along Γ–L shown in figure 2(b) of [16], with the sp gap near the Fermi energy and the onset of the d bands at -2.2 eV. In the first-layer LDOS (figures 4(c) and (d)) we would like to emphasize three features: around the centre of the first surface Brillouin zone (SBZ) ($\overline{\Gamma}$) the Shockley surface state residing in the sp gap near E_F and the Tamm-like surface resonances in the d-band region (cf [16] and references therein), and near $\overline{\mathrm{M}}$ the Tamm surface state, which was also previously observed by photoemission [26].

In order to assess to what extent pair emission spectroscopy may reflect the valence electron LDOS, we now

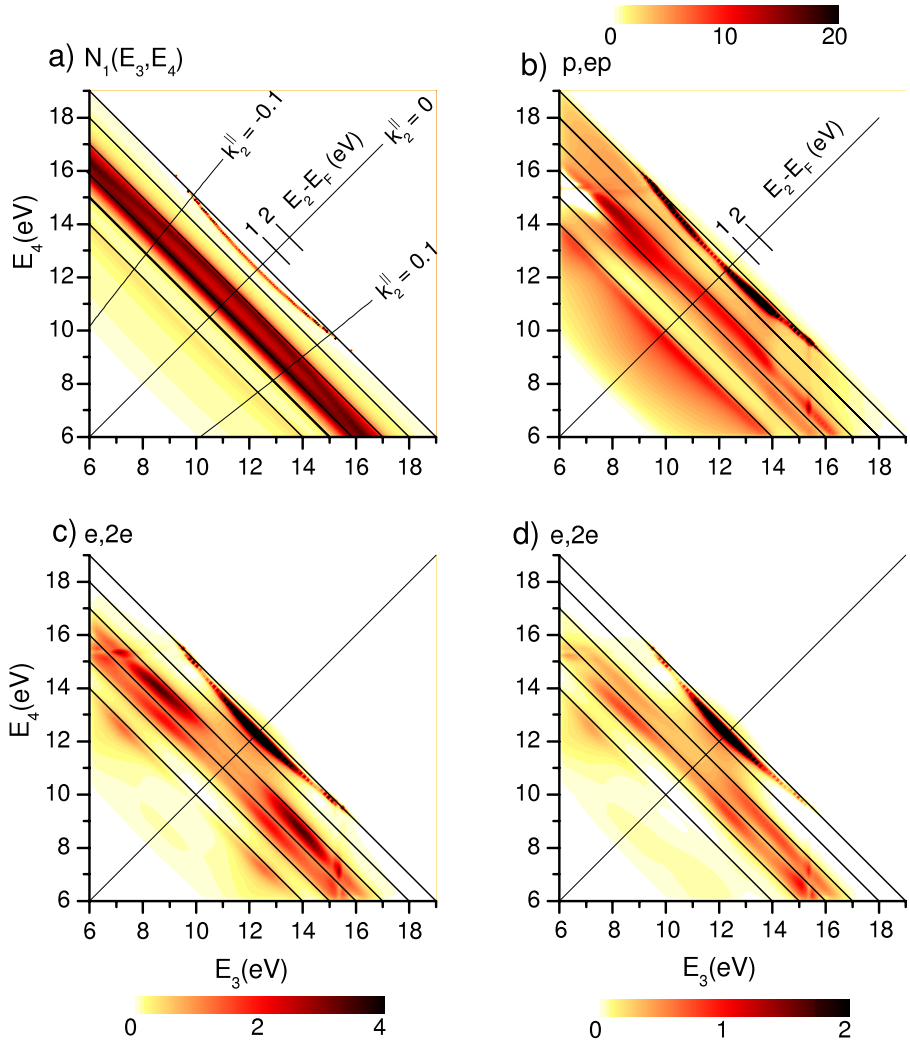

Figure 5. Pair emission spectra $I(E_3, E_4)$ from Cu(111) for coplanar symmetric set-up with normal incidence of primary positron or electron of energy $E_1 = 30$ eV and emitted particles with energies E_3 and E_4 and polar angle $\vartheta_3 = \vartheta_4 = 30°$. The reaction plane is the (x, z) plane (with x along the $[1, -1, 0]$ direction and z normal to the surface). The (y, z) plane is a mirror plane of the semi-infinite crystal. Since the SOC-induced dependence of the spectra on the spin of the primary particle is of the order of a few per cent for (e, 2e) and at least an order of magnitude smaller for (p, ep), we show here only the spectra averaged over the primary spin, i.e. for an unpolarized primary beam.
(a) First-layer valence electron density of states $N_1(E_3, E_4) = N_1(E_2, k_x; k_y = 0)$. The diagonal axis represents the valence electron energy E_2 with respect to the Fermi energy. The axis normal to it is associated with $k_x = k_2^{\parallel}$ (cf equation (7)) as indicated by the iso-$k_2^{\parallel}$ lines (in atomic units). The calculation was done with the same energy-dependent imaginary potential part (cf section 2.3), which was used for the valence electron in the (p, ep) and (e, 2e) calculations. (b) $I(E_3, E_4)$ for (p, ep). (c) $I(E_3, E_4)$ for spin-unresolved (e, 2e). (d) $I(E_3, E_4)$ for (e, 2e) with fixed anti-parallel spins of the emitted electrons.

consider a symmetric coplanar set-up with normal incidence of the primary particle (i.e. $\vec{k}_1^{\parallel} = 0$) and fixed polar angles $\vartheta_3 = \vartheta_4$ of the two emitted particles. For a given reaction plane and primary energy E_1, the (p, ep) and the (e, 2e) cross sections are then functions $I(E_3, E_4)$ of the energies of the two outgoing particles and can be represented by a contour plot in the (E_3, E_4) plane. For each pair (E_3, E_4), a pair $(E_2, \vec{k}_2^{\parallel})$ of the valence electron is determined as $E_2 = E_3 + E_4 - E_1$ and $\vec{k}_2^{\parallel} = \vec{k}_3^{\parallel} + \vec{k}_4^{\parallel} - \vec{k}_1^{\parallel}$, where $\vec{k}_2^{\parallel}$ is not restricted to the first SBZ. Thus $\vec{k}_2^{\parallel}$ is in the reaction plane, with the component

$$k_2^{\parallel} = \left(\sqrt{2E_3} - \sqrt{2E_4}\right) \sin \vartheta_3. \tag{7}$$

The $\vec{k}_2^{\parallel}$-resolved density of states $N_m(E_2, \vec{k}_2^{\parallel})$ for the mth atomic layer parallel to the surface can therefore also be represented by a contour plot in the (E_3, E_4) plane. In this plot, the diagonal $E_3 = E_4$, on which $k_2^{\parallel} = 0$, can be viewed as the E_2 axis, and the other diagonal, which marks the Fermi energy, is associated with $k_2^{\parallel}$ (with a nonlinear scale according to equation (7)).

In figure 5(a) the surface LDOS N_1 for Cu(111) is represented in this way for primary energy 30 eV and emission in the (x, z) plane at polar angles $\vartheta_3 = \vartheta_4 = 30°$. N_1 in figure 5(a) is seen to correspond to a small section (around Γ) of the surface LDOS along $\overline{\Gamma}$–$\overline{\mathrm{M}}$ shown in figure 4(c). In particular, it exhibits, near E_F, the Shockley surface state.

Prior to presenting calculated pair emission cross sections from Cu(111), we would like to address the relevance of spin–orbit coupling (SOC). SOC in valence electron states

as well as in LEED and LEPD states generally causes the (p, ep) and the (e, 2e) cross section to depend on the spin of the primary particle. Sizeable asymmetries of this nature have previously been theoretically predicted [27] and experimentally verified [9] for (e, 2e) from the large-Z material W(001). In the presently studied case of Cu(111), they are, however, quite small (of the order of a few per cent) for (e, 2e) because of the fairly low Z of Cu. For (p, ep) we found them to be even smaller, by at least an order of magnitude. To explain this, we recall that SOC effects are much smaller in LEPD than in LEED [28]. Consequently, in (p, ep) only two of the single-particle states (the outgoing electron state and the valence electron state) are significantly affected by SOC, whereas in (e, 2e) this applies to all four states. We therefore do not elaborate on SOC effects in this work and present only intensities averaged over the spin of the primary particle, which corresponds to an experiment with an unpolarized source.

The calculated (p, ep) energy distribution $I(E_3, E_4)$ for $E_1 = 30$ eV, which is associated with the surface LDOS in figure 5(a), is shown in figure 5(b), with E_3 and E_4 denoting the energies of the emitted positron and electron, respectively. For comparison, we show in figure 5(d) its counterpart for spin-resolved (e, 2e), where E_3 and E_4 refer to the emitted spin-up and spin-down electron, respectively. While a substantial valence electron LDOS is obviously a prerequisite for strong intensity features, both the Shockley surface state and the d-like states manifest themselves in the pair emission distributions in a very inhomogeneous way due to differences in the final state wavefunctions in the integrals in the intensity expression equation (1).

In the (p, ep) energy distribution (figure 5(b)), the asymmetry with respect to the diagonal, i.e. to an interchange of positron and electron energies, is immediately plausible since the final state 'fast positron, slow electron' (below the diagonal in figure 5(b)) is very different from the state 'slow positron, fast electron' (above the diagonal). The strong Shockley-derived intensity feature for the emitted positron energy between 12.5 and 14 eV can be traced back to surface resonances in the LEPD state, which are associated with the emergence threshold for two non-specular LEPD beams.

In the fixed anti-parallel spins (e, 2e) energy distribution (figure 5(d)), the Shockley surface state is seen to appear symmetrically to the 'equal-energy-sharing' diagonal, i.e. invariant to an interchange of the values of the energies E_3 and E_4. This is readily understood: the sp-like Shockley state is symmetric and the interchange does not alter the spatial part of the final two-electron state. In contrast, some of the valence d states (in the range 2–4 eV below E_F, cf figure 4) are antisymmetric, which entails an asymmetry of $I(E_3, E_4)$ in this energy range.

The spin-unresolved (e, 2e) energy distribution (figure 5(c)) is, as a consequence of exchange, the sum of a direct anti-parallel spin part I_d, which is actually the intensity shown in figure 5(d), an exchange anti-parallel spin part I_e, which is the mirror image of I_d with respect to the diagonal, and a parallel spin part I_{par}, which is mirror-symmetric (cf [6, 7]). $I(E_3, E_4)$ in figure 5(c) is therefore symmetric and, I_{par} being comparatively small, close to the sum of $I(E_3, E_4)$ in figure 5(d) and its mirror image.

In the above energy distributions at constant emission angles the valence state and the final two-particle state are varied. For the study of correlation effects between the two emitted particles, angular distributions obtained in a 'constant initial state' set-up like the one shown in figure 6(a) is more suitable. The primary particle has constant energy E_1 and surface-parallel momentum $\vec{k}_1^{\parallel}$, i.e. fixed polar and azimuthal angles of incidence (ϑ_1, φ_1). For the emitted particles we choose constant $E_3 = E_4$ and variable $\vec{k}_3^{\parallel} = -\vec{k}_4^{\parallel}$. According to energy and parallel-momentum conservation the valence state has thus a constant energy E_2 and $\vec{k}_2^{\parallel} = -\vec{k}_1^{\parallel}$. The pair emission intensity then depends only on $\vec{k}_3^{\parallel}$ or, equivalently, on (ϑ_3, φ_3).

In figure 6 we focus on the special case of normal incidence of the primary particle and consequently $\vec{k}_2^{\parallel} = 0$. Choosing further $E_1 = 30$ eV and $E_3 = E_4 = 12.3$ eV, the active valence electron is in the Shockley surface state at the centre of the SBZ with energy $E_2 = E_F - 0.4$ eV.

In figure 6(b) we show the (p, ep) angular distribution $I(\vec{k}_3^{\parallel})$ calculated for this case. As one would qualitatively expect, the intensity is largest in the centre, i.e. for small polar emission angles ϑ. The mirror symmetry with respect to the (y, z) plane and the threefold rotation symmetry about the surface normal correspond to the C_{3v} symmetry of the semi-infinite Cu(111) crystal. The (e, 2e) angular distribution for the case of fixed anti-parallel spins (figure 6(d)) also exhibits these symmetries, but only very small intensities for small emission angles. It is tempting to interpret this central depletion zone as a Coulomb correlation hole (cf figures 5 and 6 in [7]). For the present energies, however, an angular distribution calculated without Coulomb correlation already exhibits, due to matrix element effects, a depletion zone almost as pronounced as the one shown in figure 6(d).

If the spins of the two electrons are not resolved, the distribution (shown in figure 6(c)) becomes sixfold by adding to the direct anti-parallel spin part I_d an exchange anti-parallel spin part I_e, which is rotated azimuthally by 180° with respect to I_d. Further, it contains a parallel spin part I_{par}, which is inherently sixfold due to exchange.

While the occurrence of a central accumulation zone in (p, ep) as opposed to a central depletion zone in (e, 2e) appears plausible, it is striking at first glance that also further out the (p, ep) intensity is much larger than its fixed spins' (e, 2e) counterpart, e.g. for $(k_x, k_y)/k$ around (0.65, 0.4) by a factor of about 5. (Note the different scales on the colour bars.) To what extent this is due to the difference between the positron and electron single-particle states on the one hand and due to the Coulomb correlation in the emitted pair state on the other will be explored in the following.

In figure 7 we compare (p, ep) angular intensity distributions calculated, for normal incidence of a positron with energy 29 and 30 eV on Cu(111), without Coulomb correlation in the emitted pair state (by taking the correlation factor f^c (cf equation (3)) as 1) (left-hand panels) with their counterparts calculated with Coulomb correlation (by using the numerically calculated f^c) (right-hand panels). Please note that in the plots the intensity of the 'without' panels has been scaled up by a factor of two with respect to the 'with' panels.

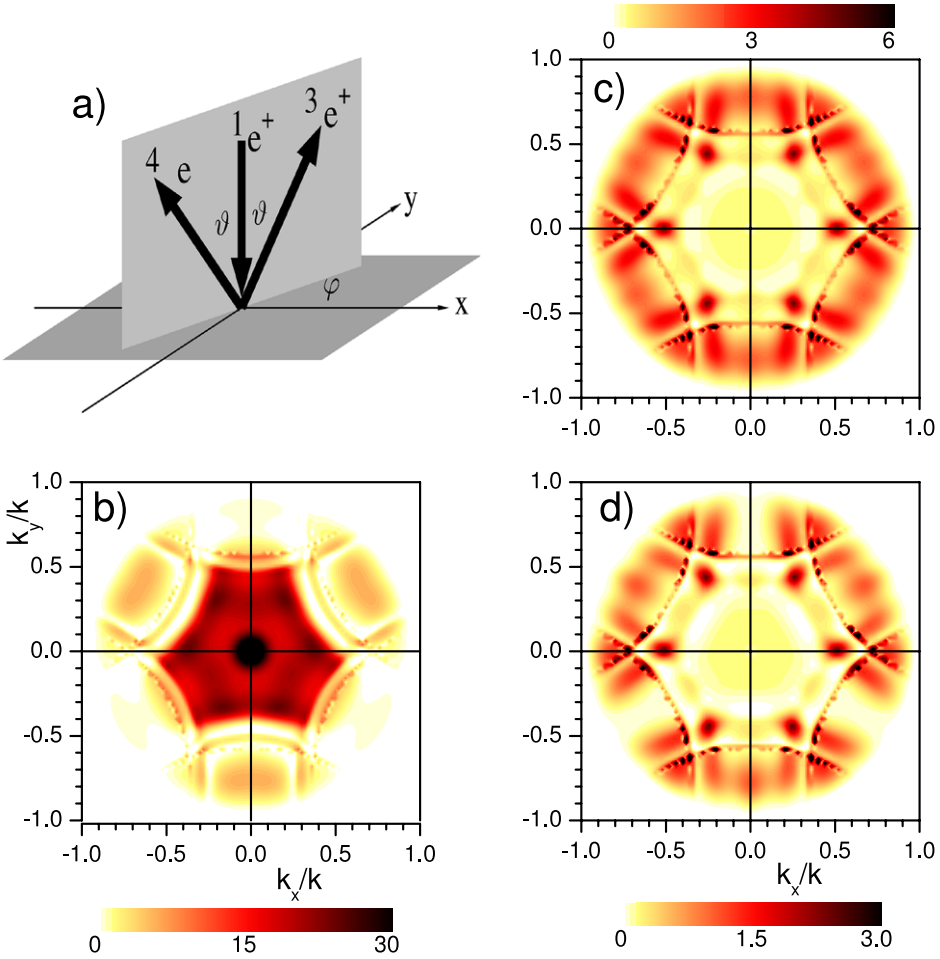

Figure 6. Angular distribution of the pair emission intensity from Cu(111) upon normal incidence of an unpolarized positron or electron beam with energy $E_1 = 30$ eV. The set-up is coplanar symmetric with fixed equal energies $E_3 = E_4 = 12.3$ eV and surface-parallel momenta $(k_3^x, k_3^y) = (-k_4^x, -k_4^y)$ of the emitted particles. The relevant valence state is thus the bottom of the Shockley surface state with energy $E_2 = E_F - 0.4$ eV and $\vec{k}_2^{\parallel} = 0$. (a) Sketch of the present (p, ep) set-up. The angles ϑ and φ determine the above surface-parallel momentum components of the emitted positron as $k_3^x = k_3 \sin\vartheta \cos\varphi$ and $k_3^y = k_3 \sin\vartheta \sin\varphi$, where $k_3 = \sqrt{2E_3} = 0.95$ Bohr^{-1}. The (e, 2e) set-up is analogous. (b) Intensity $I(k_x/k, k_y/k)$ for (p, ep), where $(k_x, k_y) := (k_3^x, k_3^y)$ and $k := k_3$. (c) Intensity $I(k_x/k, k_y/k)$ for (e, 2e) not spin-resolved. (d) Intensity $I(k_x/k, k_y/k)$ for (e, 2e) with fixed anti-parallel spins of the emitted electrons.

The most important effect of the Coulomb correlation is, as one would expect, a strong enhancement for small emission angles. An enhancement, of about a factor of two, is however also found for large emission angles. To understand this, we first note that in the intensity formula equation (1) the correlation factor $f^c(\vec{r}; \vec{k})$ (cf equation (3)) can be taken out of the final two-particle state $|3, 4\rangle$ and incorporated into the Coulomb interaction $U(\vec{r})$. This amounts to an intensity formula with a correlation-modified Coulomb potential

$$U^c(\vec{r}; \vec{k}) = f^c(\vec{r}; \vec{k}) U(|\vec{r}|) \tag{8}$$

and an uncorrelated final two-particle state. Since for the positron–electron pair $|f^c|$ is much larger than unity for small k and r (cf figures 1 and 2), a strong enhancement of the pair emission intensity at small angles is obvious. A closer inspection of $|f^c|$ as a function of the momentum difference k reveals that it is still fairly large for the maximal momentum difference in the case of figure 7, which is reached at grazing exit and amounts to $2\sqrt{2E_3} = 1.9$ Bohr^{-1}.

Returning to the above-raised question, why the 'further-out' (p, ep) intensity around $(k_x, k_y)/k = (0.65, 0.4)$ is about five times larger than the corresponding (e, 2e) intensity (cf figures 6(b) and (d)), the lower panels of figure 7 show that the electron–positron correlation is responsible for a factor of about two. On the other hand, the (e, 2e) intensity in figure 6(d), which was calculated including electron–electron correlation, is weaker by a factor of about two than its counterpart without correlation. Consequently, the Coulomb correlation is the main cause of this difference between (p, ep) and (e, 2e).

The striking differences between the (p, ep) angular distributions for primary energy 29 eV (upper panels of figure 7) and primary energy 30 eV (lower panels of figure 7) are due to numerical differences in the respective integrals in equation (1). While correlation always enhances the central region more strongly than the outer one, such 'matrix element effects' may, as in the case of $E_1 = 29$ eV, dominate, with the consequence that there is eventually a central depletion zone instead of a naively expected 'correlation hill'.

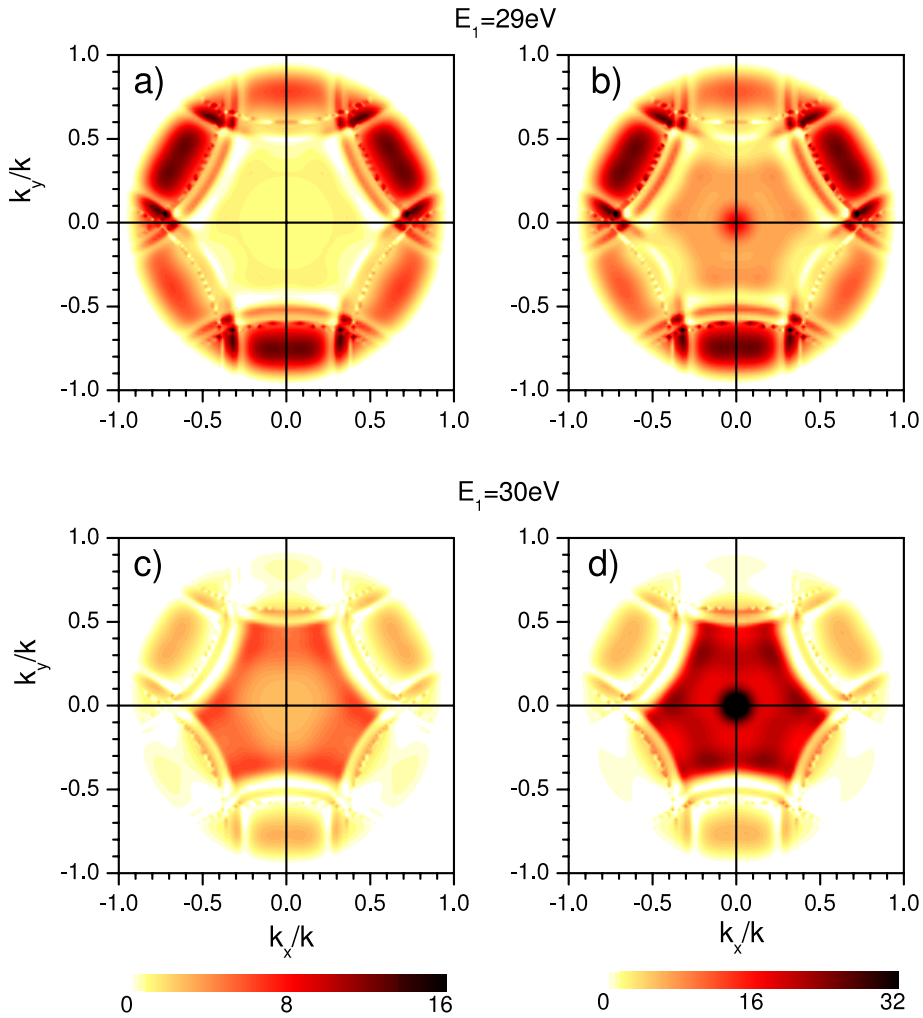

Figure 7. Correlation effect in the angular distribution of (p, ep) from Cu(111) upon normal incidence of a positron. The set-up is the same as described in the caption to figure 6, with $E_1 = 29$ eV and $E_3 = E_4 = 11.8$ eV (panels (a) and (b)), and $E_1 = 30$ eV and $E_3 = E_4 = 12.3$ eV (panels (c) and (d)), such that in both cases the electron is excited from the bottom of the Shockley surface state. The Coulomb correlation in the emitted electron–positron pair state has been neglected (by taking the correlation factor f^{c} (cf equation (3)) as 1) in the left-hand panels (a) and (c), whereas it has been included (by using the numerically calculated f^{c}) in the right-hand panels (b) and (d). Note that the intensity scale in panels (b) and (d) is twice the one in panels (a) and (c).

The (p, ep) and (e, 2e) angular distributions in figures 6 and 7 have a pronounced feature in common: the circular narrow structures, which intersect the k_x/k axis around 0.65, and those related to them by threefold rotation symmetry. These structures are manifestations of surface resonances in the LEED and LEPD states of the emitted particles, which are associated with the emergence thresholds of non-specular beams.

In the above 'constant initial state' angular intensity distributions, the relevant valence electron is at the bottom of the Shockley surface state at the centre of the surface Brillouin zone (SBZ). In the following we consider analogous (p, ep) angular distributions, which are associated with valence electron states further out in the SBZ. Since parallel-momentum conservation implies $\vec{k}_2^{\parallel} = -\vec{k}_1^{\parallel} + \vec{g}^{\parallel}$, a specific valence electron state can be selected by off-normal incidence of the primary particle with an appropriate $\vec{k}_1^{\parallel}$.

Two typical examples of the resulting (p, ep) angular distributions are shown in figure 8, for a 30 eV positron incident with azimuthal angle $\varphi_1 = 90°$, i.e. in the (y, z) mirror plane, and polar angle ϑ_1. Thus $\vec{k}_1^{\parallel} = (0, k_1^y) = (0, -\sqrt{2E_1}\sin\vartheta_1)$ and $\vec{k}_2^{\parallel} = (0, k_2^y) = (0, -k_1^y + g^y)$, where we choose the reciprocal lattice vector component g^y such that $\vec{k}_2^{\parallel}$ is in the first SBZ. The emitted particle energies are chosen, like in the previous examples, as $E_3 = E_4 = 12.3$ eV, which implies $E_2 = E_{\mathrm{F}} - 0.4$ eV.

In the first example, a valence state with $k_2^y = 0.67$, i.e. associated with a high sp-like bulk density (cf figure 4), is selected by choosing the angle of incidence $\vartheta_1 = 26.5°$. The resulting (p, ep) angular distribution (figure 8(a)), which is necessarily mirror symmetric with respect to the (y, z) plane, exhibits, like in the above normal incidence case, a central accumulation zone due to the Coulomb correlation in the emitted electron–positron pair. Also, further out the circular structures due to LEPD and LEED surface resonances are present, but with a much stronger weight on the feature around $k_y/k = -0.6$, i.e. with $k_3^y = k_y = -0.57$, which is near to $k_1^y = -0.67$ of the primary positron.

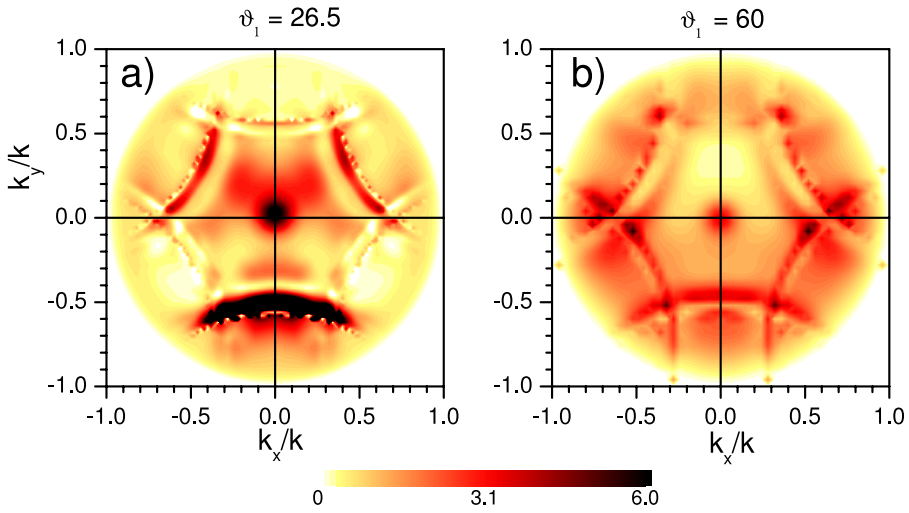

Figure 8. Angular distribution of (p, ep) from Cu(111) for off-normal incidence of a positron with $E_1 = 30$ eV. The emission set-up is the same as described in the caption to figure 6. The positron is incident in the (y, z) plane at polar angle $\vartheta_1 = 26.5°$ (panel (a)) and $\vartheta_1 = 60°$ (panel (b)). According to energy and momentum conservation, the valence electron thus has energy $E_2 = E_F - 0.4$ eV in both cases, and surface-parallel momentum $(k_2^x = 0, k_2^y)$ with $k_2^y = 0.67$ Bohr^{-1} for $\vartheta_1 = 26.5°$ and $k_2^y = 0.21$ Bohr^{-1} for $\vartheta_1 = 60°$.

For the larger angle of incidence $\vartheta_1 = 60°$, we have $k_1^y = -1.29$, which upon addition of the reciprocal lattice vector component $g^y = 1.50$ yields for the valence electron $k_2^y = 0.21$. We recall from above that $E_2 = E_F - 0.4$ eV. From figure 4 this valence state is seen to be in a region of very low sp-like density of states. The corresponding (p, ep) angular distribution is shown in figure 8(b). We notice again the circular structures and a central Coulomb correlation hill, which is however weaker than the one in figure 8(a).

Our finding that the central correlation hill and the circular structures are fairly similar for different initial states and identical final states is due to the fact that they are basically final state features arising from the electron–positron Coulomb correlation and LEPD/LEED surface resonances, respectively.

4. Concluding remarks

Loosely speaking, the positron–electron Coulomb correlation is stronger than the electron–electron Coulomb correlation. We have demonstrated this firstly for the pair correlation function between two plane-wave particles coupled by a screened or bare Coulomb interaction and secondly for the single-particle potential describing the interaction with the solid, the correlation part of which, while negative for both positron and electron, is about six times larger in magnitude for the positron. As a consequence of the latter, the total inner potential (at low energies) for the positron is also negative despite the repulsive nature of the electrostatic Hartree potential part.

While (p, ep) energy distributions for constant emission angles reflect, to a large extent, the valence electron density of states, equal-energy angular distributions for a fixed initial two-particle state are most suitable for studying Coulomb correlation effects. The latter tend to manifest themselves in (p, ep) as a central accumulation zone ('correlation hill'), as opposed to a central depletion zone ('correlation hole') in (e, 2e). Comparison with results, which we obtained without Coulomb correlation in the emitted pair, shows, however, that the relative intensity and extension of this central zone can be strongly influenced by 'matrix element effects'. Caution is therefore required in viewing an observed central hill or hole as a correlation feature. Further out, both the (p, ep) and the (e, 2e) angular distributions exhibit narrow circular structures, which arise from surface resonances in the outgoing (time-reversed) LEED and LEPD states.

For Cu(111), we found the SOC-induced dependence on the spin of the primary particle to be a few per cent for (e, 2e), and by at least an order of magnitude smaller for (p, ep), since LEPD states are much less affected by SOC than LEED states. We have therefore only shown intensities averaged over the primary spin, which applies to an experiment with an unpolarized source.

For ferromagnets, the dependence of the (p, ep) intensity on the primary spin differs more fundamentally from that in (e, 2e). While SOC produces an asymmetry in both cases (which for 3d ferromagnets should be comparable to what we presently obtained for Cu), the exchange-induced spin dependence, which is sizeable in (e, 2e) (cf [5, 6, 8] and references therein), is entirely absent in (p, ep), since positron and electron are distinguishable particles. In principle, dipole–dipole interaction between the incident particle and the valence electron may lead to a further spin dependence of (p, ep) and (e, 2e), which should, however, be extremely small.

Acknowledgments

We are grateful to S Bluegel and G Bihlmaier for making their FLAPW package FLEUR available to us and for providing us with valuable help in using it. Further, we are pleased to acknowledge stimulating discussions with J Kirschner and F O Schumann at the Max-Planck-Institute of Microstructure Physics in Halle.

References

[1] Schultz P J and Lynn K G 1988 *Rev. Mod. Phys.* **60** 701
[2] Puska M J and Nieminen R M 1994 *Rev. Mod. Phys.* **66** 841
[3] Coleman P G 2002 *Appl. Surf. Sci.* **194** 264
[4] van Riessen G A, Schumann F O, Birke M, Winkler C and Kirschner J 2008 *J. Phys.: Condens. Matter* **20** 442001
[5] Feder R and Gollisch H 2003 *Solid State Photoemission and Related Methods* ed W Schattke and M A Van Hove (Weinheim: Wiley–VCH)
[6] Ruecker U, Gollisch H and Feder R 2005 *Phys. Rev.* B **72** 214424
[7] Gollisch H, Schwartzenberg N V and Feder R 2006 *Phys. Rev.* B **74** 075407
[8] Samarin S, Berakdar J, Artamonov O M and Kirschner J 2000 *Phys. Rev. Lett.* **85** 1746
[9] Samarin S, Artamonov O M, Sergeant A D, Kirschner J, Morozov A and Williams J F 2004 *Phys. Rev.* B **70** 073403
[10] Schumann F O, Kirschner J and Berakdar J 2005 *Phys. Rev. Lett.* **95** 117601
[11] Schumann F O, Winkler C and Kirschner J 2007 *New J. Phys.* **9** 372
[12] Berakdar J 2000 *Nucl. Instrum. Methods Phys. Res.* B **171** 204
[13] See www.flapw.de
[14] Vosko S H, Wilk L and Nusair M 1980 *Can. J. Phys.* **58** 1200
[15] Huefner S 2003 *Photoelectron Spectroscopy* (Berlin: Springer)
[16] Courths R, Lau M, Gollisch H, Scheunemann T and Feder R 2001 *Phys. Rev.* B **63** 195110
[17] Samarin S N, Williams J F, Sergeant A D, Gollisch H and Feder R 2007 *Phys. Rev.* B **76** 125402
[18] Boev O V, Puska M J and Nieminen R M 1987 *Phys. Rev.* B **36** 7786
[19] Fazleev N G, Fry J L and Weiss A H 1998 *Phys. Rev.* B **57** 12506
[20] Arponen J and Pajanne E 1979 *Ann. Phys.* **121** 343
[21] Boronski E and Nieminen R M 1986 *Phys. Rev.* B **34** 3820
[22] Boronski E and Stachowiak H 2001 *Phys. Rev.* B **57** 6215
[23] Lambrick D B and Siopsis G 1982 *Surf. Sci.* **120** L491
[24] Jona F, Jepsen D W, Marcus P M, Rosenberg I J, Weiss A H and Canter K F 1980 *Solid State Commun.* **36** 957
[25] Oliva J 1980 *Phys. Rev.* B **21** 4909
[26] Heimann P, Hermanson J, Miosga H and Neddermeyer H 1979 *Phys. Rev.* B **20** 3059
[27] Gollisch H, Scheunemann T and Feder R 1999 *J. Phys.: Condens. Matter* **11** 9555
[28] Feder R 1980 *Solid State Commun.* **34** 541